





Studying the spatial structure of urban heat exposure in Berlin utilising Moran drop plots and seismograms

René Westerholt ^{1,*} and Florian Klopfer ^{1,*}

¹Department of Spatial Planning, TU Dortmund University, Dortmund, Germany

*These authors contributed equally to this work.

Correspondence: René Westerholt (rene.westerholt@tu-dortmund.de)

Abstract. Both the degree of urbanisation and climate change are continuing to accelerate. As a result, heat islands in cities are an increasing problem. In this article, we analyse a dataset of land surface temperatures in Berlin. The heat information is not mapped on administrative or census units, but summarised into so-called urban structure type units. These are not only meaningful in terms of their inherent link to urban heat but also represent a geography that is relevant for planning purposes. Our analysis complements existing studies in Berlin by applying two novel visual spatial analysis methods: the Moran drop plot and the Moran seismogram. These allow structures to be visually explored that are not found in traditional Moran scatterplots. In this way, we can visualise that low-temperature areas tend to be more homogeneously clustered than their high-temperature counterparts. In turn, the latter can be identified in the plots as clearly smaller in geographic scale and thus as more heterogeneous in the neighbourhoods formed. Finally, we draw conclusions including possible policy-relevant considerations.

Keywords. urban heat, land surface temperatures, spatial analysis, urban planning, Moran scatterplot

1 Introduction

Urban heat islands (UHI) are evident in many cities. Oke (1982) defines an urban heat island as a thermal anomaly that has both vertical and horizontal dimensions. The intensity of an UHI is determined by the difference between the temperatures in the city and a corresponding rural reference area (Hsu et al., 2021). The effects of urban heat islands depend both on characteristics of the urban environment, such as the size of a built-up area, population, building density, and land use distribution, and on external factors such as climate, weather profiles, and the seasons (Oke, 1982). The Intergovernmental Panel on Climate Change (IPCC) lists various health effects caused

by heat in cities and also presents evidence that increased temperatures contribute significantly to productivity losses (IPCC, 2022). In addition, the increased mortality rate associated with urban heatwaves is well documented worldwide (Massetot et al., 2023; Winklmayr et al., 2022). However, heat exposure in cities is not evenly distributed. The intensity of heat islands is often characterised by spatial inequalities to the detriment of less affluent or otherwise disadvantaged city dwellers (Hoffman et al., 2020; Hsu et al., 2021; Mitchell et al., 2021). Also for Berlin, the case study that we look at in this paper, a recent study suggests that poorer households suffer unduly from the effects of urban heat islands (Chakraborty et al., 2019).

Climate change and all its effects will continue to progress. It is estimated that children born in 2020 will have to endure adverse events such as heatwaves two to seven times more often in their lives than people born in 1960 (Thiery et al., 2021). This is not surprising when considering that Berlin, for example, by 2070, is predicted to have a climate comparable to that of Rome today (Crespi et al., 2023). In addition, urbanisation is another ongoing process with annual urban population growth rates of 0.5% for high-income regions and 4.1% (both figures from 2022) for low-income regions (World Bank, 2022). By 2025, 68.4% of the world's population is expected to live in agglomerations (UN Department of Economic and Social Affairs, 2019). Time series analyses show a strong global increase in UHI extremes for the period 2003–2020 and link this to the aforementioned processes of advancing urbanisation and accelerating climate change, indicating an overall intensification of urban climate challenges in the future (Mentaschi et al., 2022).

In the present study, we follow the established approach of relying on land surface temperatures to identify urban heat islands and to quantify their intensity and thus the heat exposure of city dwellers (c.f., Chakraborty et al., 2019; Hsu et al., 2021). The influence of urban structures on temperature has been widely researched, with factors such as imperviousness (Yuan and Bauer, 2007) and urban

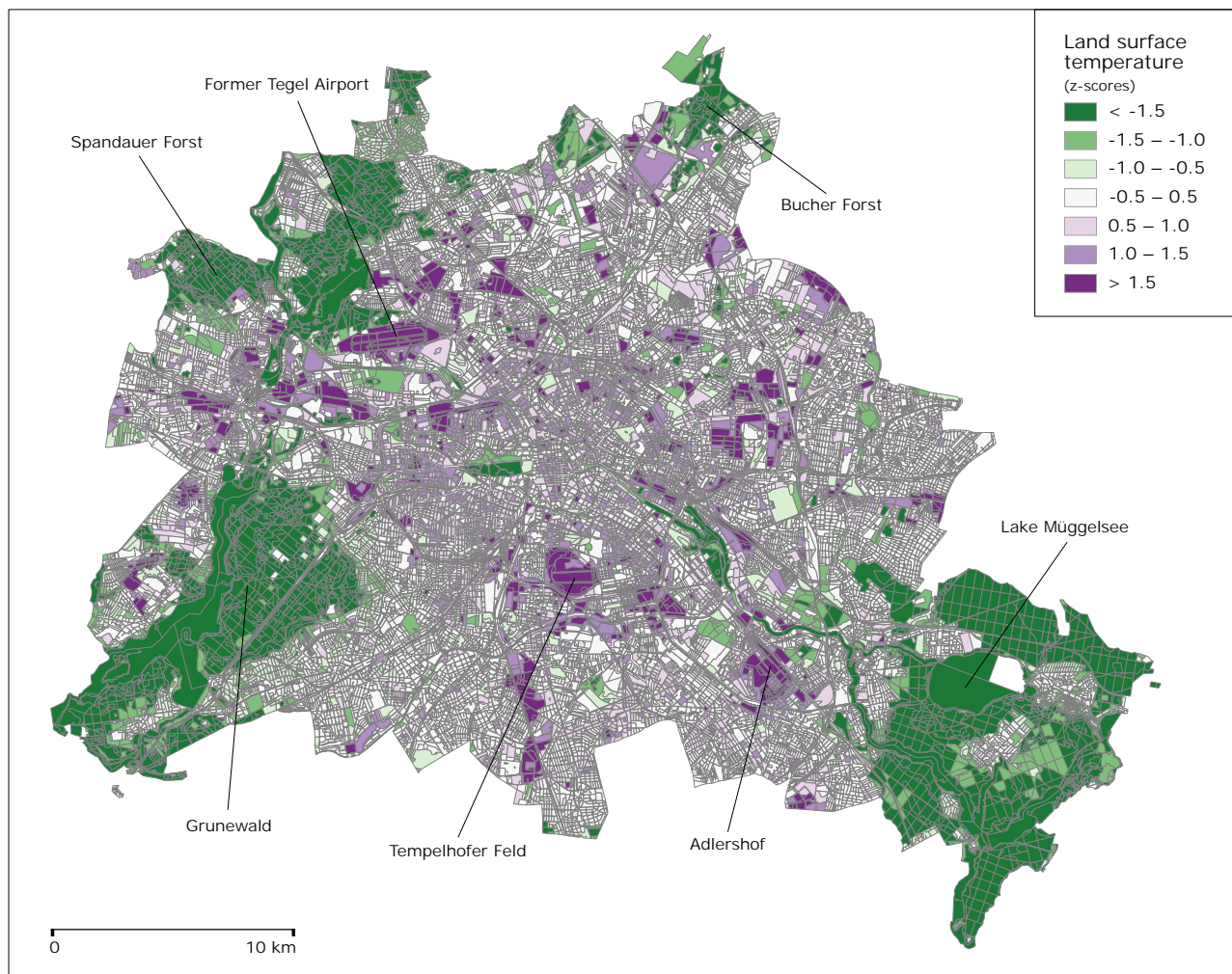


Figure 1. Mapped land surface temperatures in Berlin. The values are standardised and therefore given as z-scores.

greening (Mitchell et al., 2021), but also urban morphology, being studied at a more general level, for example using the concept of so-called local climate zones (Stewart and Oke, 2012). For this study, the spatial aggregation used is the level of so-called urban structure types, which were defined for the city of Berlin to represent homogeneous urban structures based on typical building and open space characteristics (Senatsverwaltung für Stadtentwicklung, Bauen und Wohnen, 2021).

2 Data and methods

The following two subsections present the data and methods employed in this paper. First, we present our Berlin dataset before introducing the three types of visual analysis instruments used for our spatial analysis.

2.1 Data

The urban structure type dataset and the administrative boundaries were obtained from the Berlin Senate De-

partment for Urban Development, Building, and Housing (Senatsverwaltung für Stadtentwicklung, Bauen und Wohnen, 2021). Landsat 8 scenes with a spatial resolution of 30×30 m were additionally used to derive the land surface temperatures and come from USGS's Earth Explorer platform¹. For the calculation of land surface temperatures from the remote sensing imagery, we use the approach presented by Avdan and Jovanovska (2016). To ensure a robust approximation of the thermal conditions and to avoid the erroneous adoption of local maxima from any particular year, we combine three Landsat scenes recorded on three hot days (maximum temperature above 30°C as defined by the German Meteorological Service²) in different years (2019, 2020 and 2022) and without precipitation two days prior, as described in more detail by Klopfer (2023). Finally, we aggregate the temperature data to the structure type level by assigning each feature the average temperature for the area covered (see Figure 1).

¹<https://earthexplorer.usgs.gov/>; last accessed on 21 January 2024.

²https://www.dwd.de/EN/ourservices/germanclimateatlas/explanations/elements/_functions/faqkarussell/heissetage.html; last accessed on 21 January 2024

2.2 Methods

Our methodological approach employs two novel types of visual analysis techniques. Both are based on the Moran scatterplot (see Figure 2a), which has become an established exploratory analysis tool. The Moran scatterplot contrasts the spatial lags of an attribute, that is, spatially weighted and summed neighbourhoods, with the attribute values mapped at the corresponding reference locations for which those neighbourhoods are defined (Anselin, 1996). The resulting scatter then represents local and global spatial autocorrelation as measured through Moran's I (Westerholt, 2022; Getis, 2010). The first and third quadrants of the plot show positive, while the second and fourth quadrants visualise negative local spatial autocorrelation. Global autocorrelation is indicated by the slope of the trend line drawn on top of the scatterplot.

The two analysis methods used beyond the basic Moran scatterplot are variants of the latter that have recently been introduced (Westerholt, 2024): the Moran drop plot and the Moran seismogram. The drop plot is based on the coordinates of the critical values in the Moran scatter plot, but emphasises the strength of local autocorrelation patterns. The latter is achieved by highlighting all observations identified as significant and then connecting them to the coordinates of the critical values by lines that literally 'drop down' (or 'rise up'), which is illustrated in Figure 2b. The longer these lines, the higher the corresponding p values. This type of visualisation makes it possible to investigate potential regularities and trends in the interplay between attribute values, spatial lags, local configuration of spatial weights, and p values. In our current case, we use this technique to identify potential trends in the strength of spatial patterns across the attribute value range of the detected land surface temperatures. The scatterplot coordinates of the critical values can be derived from the equation of the Moran's I z-scores. The spatial lag that would be needed to obtain the respective critical value given some observed attribute value x_i is given as

$$b_i | x_i = \frac{s^2 \left(C_i \cdot \sqrt{\text{Var}[I_i]} + E[I_i] \right)}{(x_i - \bar{x})}, \quad (1)$$

where \bar{x} is the sample mean and s^2 is the estimated attribute variance, and $E[\cdot]$ and $\text{Var}[\cdot]$ are the expectation and variance operators.

The second visualisation method used is the Moran seismogram (see Figure 2c), which allows the visualisation of the coordinate tuples for the critical values of the local Moran's I values for each individual site. Two line graphs are displayed that connect the coordinates of the critical values over the course of the attribute value range above and below the mean value of the attribute. From this it becomes evident for each location whether the observed values are above or below their critical values and, more importantly, whether there are any spiky, protruding critical outlier values. The latter may suggest structural anomalies

in the underlying spatial weights and could therefore be indicative of potential misspecification in the modelled spatial layout. In this way, we can identify new potential for further research into the nexus of surface temperatures and urban structure and critically assess and add another perspective to the results presented by, for example, Klopfer (2023) and Chakraborty et al. (2019). Our parameterisation with respect to spatial weights follows the approach of Klopfer (2023) and we therefore use all visual methods presented above with k -nearest-neighbour weights with $k = 8$.

3 Results

Our visual results show a number of interesting findings that complement the results of previous studies on land surface temperature in Berlin and can inform similar studies from other cities. Figure 3a shows a basic Moran scatterplot of our land surface temperature values. Two groups of points can be recognised in this diagram: one in the first quadrant and one in the third quadrant. The group in the first quadrant is larger and reflects the built structures throughout the city, including residential, commercial, and industrial areas. Land surface temperatures in these areas are higher than average, which is reflected by the cluster being located in the 'high-high' quadrant. The other cluster in the third quadrant ('low-low') reflects the fact that Berlin includes several extensive greenspaces within its borders, such as the Grunewald in the southwest, the Spandauer Forst in the northwest, the Bucher Forst in the north, and the forests around Lake Müggelsee in the east. These form clusters with low values, and the clustering in the Moran scatterplot shows that these behave similarly in terms of their spatial organisation, as no structural breaks are visible in this cluster. Beyond these individual clusters, the scatterplot indicates strong positive spatial autocorrelation, which is to be expected for land surface temperatures.

The Moran drop plot shown in Figure 3b shows a number of findings. In general, the plot makes it clear that the Moran scatterplot visualises two different themes: global and local Moran's I . While the standard scatterplot tempts the viewer to relate the diagonal line (global) to the points (local) by their mutual distance, the drop plot, by breaking this supposed relationship, makes it very clear that the local points are to be evaluated by their own critical values instead. Beyond this general observation, there is a clear difference between clusters of low and high values, which behave differently in terms of their spatial structuring. The drops for the low values associated with the large greenspaces show a stable trend in the overall shape of the drop lines. The lower the attribute values, the longer the lines become, suggesting consistent, homogeneous clusters of low values. Visual inspection of the respective locations in the map (Figure 1) confirms this finding, as the greenspaces mentioned above are subdivided into a number of spatial units and therefore form relatively homo-

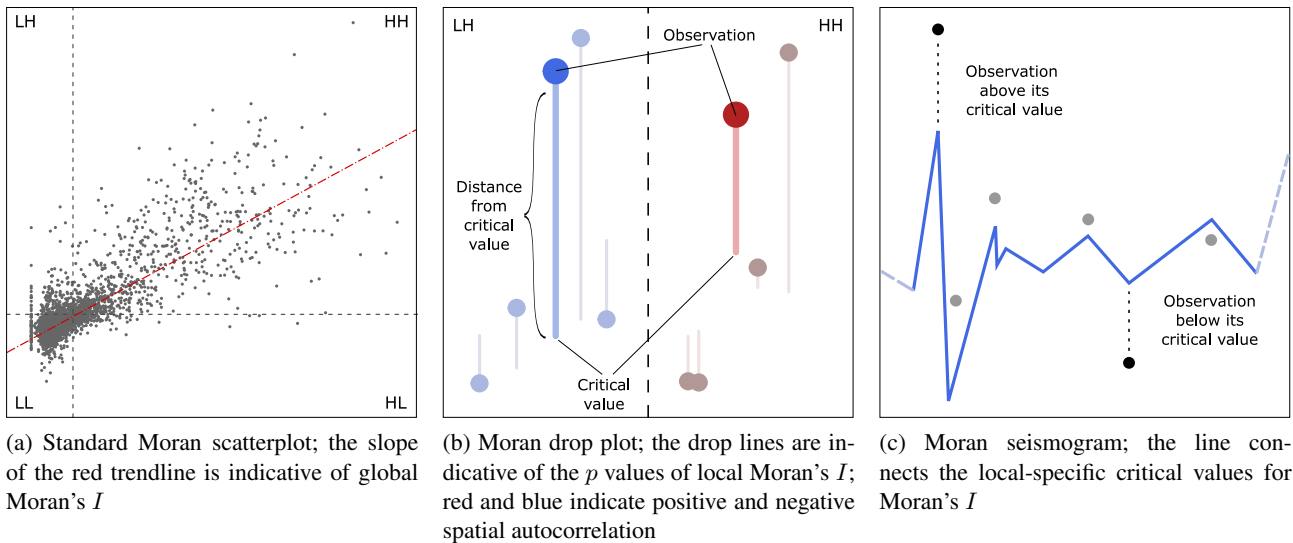


Figure 2. Illustration of the three types of Moran scatterplots used in this work. The two-character abbreviations indicate the following types of spatial associations: HH = high–high, HL = high–low, LL = low–low, LH = low–high.

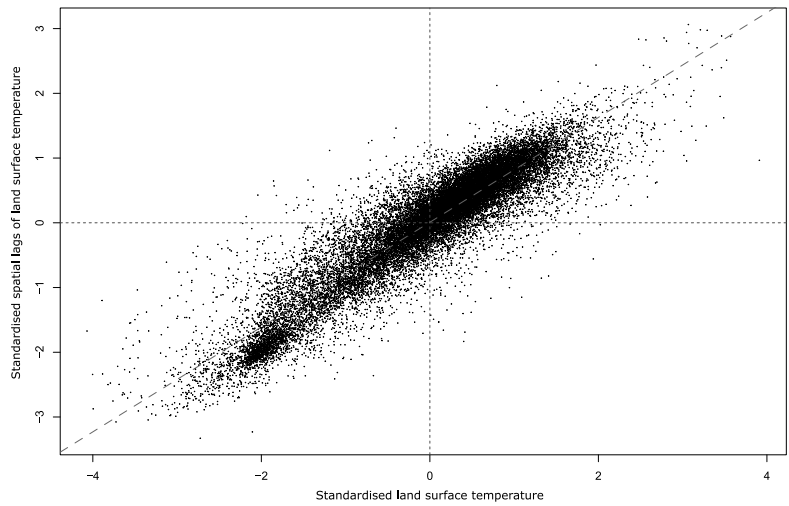
geneous neighbourhoods. This detailed sub-structuring is based on the fact that the main foundation for the USTs is the block-level geography of Berlin (Senatsverwaltung für Stadtentwicklung, Bauen und Wohnen, 2021). The shape of the clusters of high values, on the other hand, is twofold. The basic shape of the drops in the first quadrant shows an increasing flattening the higher the land surface temperature values become. In addition, there are strong outliers with long drop lines beyond attribute z -scores of about 2. The flattening shape indicates that the clusters with high values are less homogeneous than their counterparts with low values, which can be partly explained by their smaller geometric scale in the map. The outliers are mostly associated with salient locations such as the former Tegel and Tempelhof airports and the Adlershof Science and Technology Park. Low–high and high–low clustering as depicted in quadrants two and four do not exhibit noteworthy patterns in the drop plot. Checking the respective areas on the land surface temperature map reveals that such clusters are found around smaller green or blue infrastructure elements in urban, central contexts where they correspond to transition areas separating higher from lower temperatures. The drop plot thus provides clues for research into land surface temperature characteristics that would not be recognisable from the basic Moran scatterplot.

The third visualisation is the seismogram shown in Figure 3c. The seismogram features the hypothetical positions of the critical values for each location in the Moran scatterplot. The visualisation in Figure 3c shows that the present Berlin dataset in combination with the adjusted spatial weights is very uniform and does not reveal any strong outliers in geometrical or topological terms. Instead, the two lines above and below the mean for the spatial lags indicate that the critical values oscillate within fairly limited ranges, and the flattening of this oscillation towards the tails on both sides is only an effect of the smaller num-

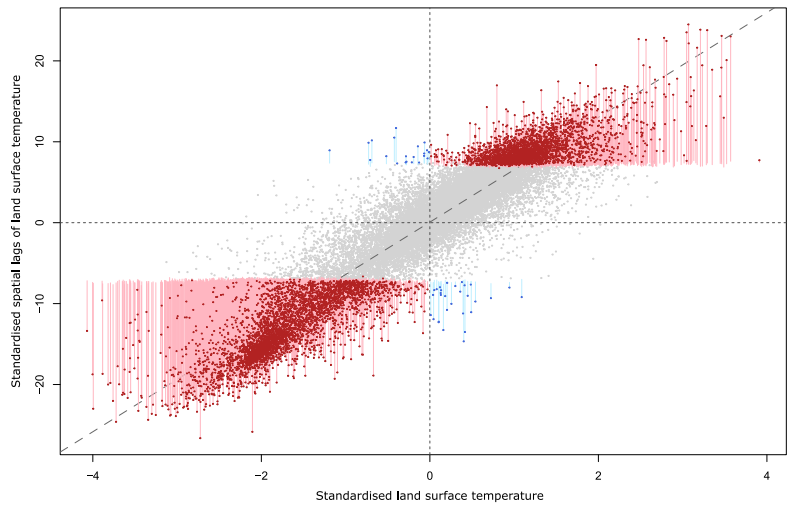
ber of data points available in these parts of the graph. The latter also confirms our finding above that the drop plot indicates heterogeneous (high-value clusters) and homogeneous (low-value) clusters in terms of the attribute values they contain. If the spatial trends evident in Figure 3c were instead due to systematic problems in the spatial organisation of the underlying units or the weights used, the seismogram would indicate this by containing corresponding deflections. Following the idea of an actual seismogram, it would then have warned us of problems. We do thus not have to assume systematic problems in the specification of our study and, in the given case of nearest-neighbour weights, can conclude that our approach is not sensitive to (at least moderate) changes in the number of neighbours (k). The latter has also been validated through testing various neighbourhood sizes ($k = 6, 10, 16, 32$) beyond $k = 8$ in the process of calculating weights, which did not result in major substantial changes of the observed structures in any of our plots. The only notable change is an increase in the number of significant spatially negatively autocorrelated observations with increasing k , which is an effect of progressively more heterogeneous neighbourhoods – and thus to be expected.

4 Conclusions

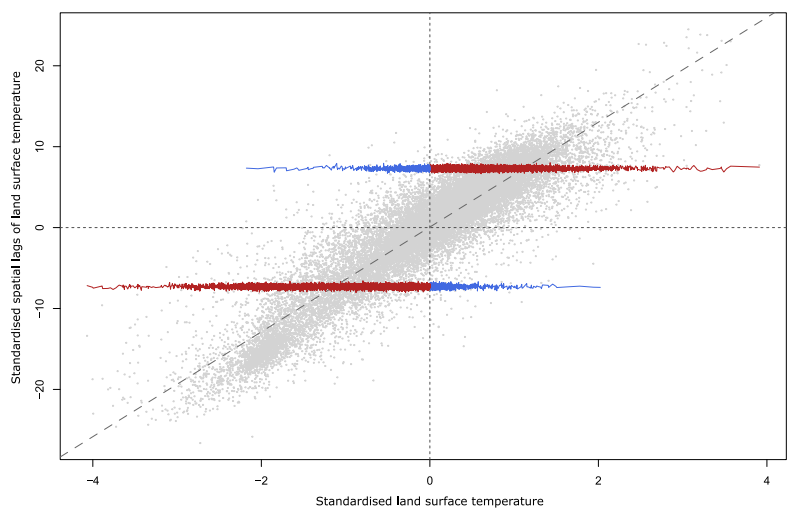
In this contribution, we have applied the traditional Moran scatterplot and two novel variants of the latter to land surface temperature values from Berlin mapped to units representing homogeneous urban structure types. The results show evidence of spatial homogeneity in areas characterised by low temperatures, such as large greenspaces. Furthermore, the visual-analytical approach revealed that, in contrast to the areas with low temperatures, above a certain point high values are no longer surrounded by



(a) Basic Moran scatterplot



(b) Moran drop plot; the lines connect observations to their critical values



(c) Moran seismogram; the lines connect the local critical values for Moran's I

Figure 3. Three types of Moran scatterplots of the Berlin land surface temperature values. The diagonal dashed trend line provides an indication of the global Moran's I . Red and blue indicate positive and negative spatial autocorrelation respectively.

equally high values in their respective neighbourhoods, though they still form significant high–high clusters. Both results point to interesting exploratory findings in the interplay between operationalisation (i.e., the units and scale of analysis) and nature of the process at hand (i.e., the mapping of land surface temperatures to urban structure type units). The units, defined by morphological and land use parameters, represent a heat-relevant urban structural aspect, but also lead to the subdivision of otherwise homogeneous areas (such as the greenspaces), resulting in different characterisations of the results obtained at both ends of the value spectrum. Obtaining these indications would not have been possible with the basic Moran scatterplot, which emphasises the usefulness of using the two proposed novel visual analysis tools.

The findings presented above can be used to derive specific recommendations for climate adaptation and urban resilience planning. In the context of our case study on land surface temperature patterns in Berlin at the spatial level of urban structure types, knowing of the type and heterogeneity of temperature clusters enables locally explicit interventions and planning. On the one hand, the homogeneous, highly significant low-temperature areas identified, which consist predominantly of green and blue infrastructures, not only require fewer temperature mitigation measures, but can also be considered potentially more resilient to changes in their surroundings. On the other hand, the highly impervious high-temperature clusters, which are often located in densely built-up urban areas, require measures to increase thermal comfort and could be prioritised for adaptation measures. The analyses presented may help in deciding which measures to take, with a focus on the transition areas between different cluster types.

Research on the relationship between urban morphology and the UHI effect (Klopfner, 2023) as well as research on social disparities in heat exposure (Chakraborty et al., 2019) and thermal justice in general may benefit from the use of an enhanced standard spatial-statistical visualisation device, as carried out and demonstrated in our study. Our approach provides a means to diagnose and improve the specification of (spatial) regression models for explaining heat patterns. In addition, the visual approach utilised may enhance future studies assessing the thermal performance of a city by allowing to better grasp the phenomenon in its entirety and in relation to different kinds of urban form. Further, from a methodological perspective, we followed the modelling approach put forward by Klopfner (2023). However, in order to increase the conclusiveness of the available results, the application and comparison of different methods of neighbourhood formation to determine spatial weights, such as contiguity or distance-based approaches, or the use of further aggregation levels could be considered in future research.

References

- Anselin, L.: The Moran scatterplot as an ESDA tool to assess local instability in spatial association, in: *Spatial analytical perspectives on GIS*, edited by Fischer, M. M., Scholten, H., and Unwin, D., pp. 111–125, Routledge, London, UK, 1996.
- Avdan, U. and Jovanovska, G.: Algorithm for automated mapping of land surface temperature using LANDSAT 8 satellite data, *Journal of Sensors*, 2016, 1480307, <https://doi.org/10.1155/2016/1480307>, 2016.
- Chakraborty, T., Hsu, A., Manya, D., and Sheriff, G.: Disproportionately higher exposure to urban heat in lower-income neighborhoods: a multi-city perspective, *Environmental Research Letters*, 14, 105003, <https://doi.org/10.1088/1748-9326/ab3b99>, 2019.
- Crespi, A., Renner, K., Zebisch, M., Schauser, I., Leps, N., and Walter, A.: Analysing spatial patterns of climate change: climate clusters, hotspots and analogues to support climate risk assessment and communication in Germany, *Climate Services*, 30, 100373, <https://doi.org/10.1016/j.cliser.2023.100373>, 2023.
- Getis, A.: Spatial Autocorrelation, in: *Handbook of Applied Spatial Analysis*, edited by Fischer, M. M. and Getis, A., pp. 255–278, Springer, Heidelberg, Germany, https://doi.org/10.1007/978-3-642-03647-7_14, 2010.
- Hoffman, J. S., Shandas, V., and Pendleton, N.: The effects of historical housing policies on resident exposure to intra-urban heat: a study of 108 US urban areas, *Climate*, 8, 12, <https://doi.org/10.3390/cli8010012>, 2020.
- Hsu, A., Sheriff, G., Chakraborty, T., and Manya, D.: Disproportionate exposure to urban heat island intensity across major US cities, *Nature Communications*, 12, 2721, <https://doi.org/10.1038/s41467-021-22799-5>, 2021.
- IPCC: Climate change 2022: impacts, adaptation and vulnerability – Working group II contribution to the sixth assessment report of the Intergovernmental Panel on Climate Change, last accessed on 21 January 2024, https://report.ipcc.ch/ar6/wg2/IPCC_AR6_WGII_FullReport.pdf, 2022.
- Klopfner, F.: The thermal performance of urban form – an analysis on urban structure types in Berlin, *Applied Geography*, 152, 102890, <https://doi.org/10.1016/j.apgeog.2023.102890>, 2023.
- Masselot, P., Mistry, M., Vanoli, J., Schneider, R., Lungman, T., Garcia-Leon, D., Ciscar, J.-C., Feyen, L., Orru, H., Urban, A., Breitner, S., Huber, V., Schneider, A., Samoli, E., Stafoggia, M., de’Donato, F., Rao, S., Armstrong, B., Nieuwenhuijsen, M., Vicedo-Cabrera, A. M., and Gasparrini, A.: Excess mortality attributed to heat and cold: a health impact assessment study in 854 cities in Europe, *The Lancet Planetary Health*, 7, e271–e281, [https://doi.org/10.1016/S2542-5196\(23\)00023-2](https://doi.org/10.1016/S2542-5196(23)00023-2), 2023.
- Mentaschi, L., Duveiller, G., Zulian, G., Corbane, C., Pesaresi, M., Maes, J., Stocchino, A., and Feyen, L.: Global long-term mapping of surface temperature shows intensified intra-city urban heat island extremes, *Global Environmental Change*, 72, 102441, <https://doi.org/10.1016/j.gloenvcha.2021.102441>, 2022.
- Mitchell, B. C., Chakraborty, J., and Basu, P.: Social inequities in urban heat and greenspace: analyzing climate justice in Delhi, India, *International Journal of*

- Environmental Research and Public Health, 18, 4800, <https://doi.org/10.3390/ijerph18094800>, 2021.
- Oke, T.: The energetic basis of the urban heat island, Quarterly Journal of the Royal Meteorological Society, 108, 1–24, <https://doi.org/10.1002/qj.49710845502>, 1982.
- Senatsverwaltung für Stadtentwicklung, Bauen und Wohnen: Umweltatlas Berlin: Stadtstruktur – Flächentypen differenziert, last accessed on 18 January 2024, <https://www.berlin.de/umweltatlas/nutzung/stadtstruktur/2020/zusammenfassung/>, 2021.
- Stewart, I. and Oke, T.: Local climate zones for urban temperature studies, Bulletin of the American Meteorological Society, 93, 1879–1900, <https://doi.org/10.1175/BAMS-D-11-00019.1>, 2012.
- Thiery, W., Lange, S., Rogelj, J., Schleussner, C.-F., Gudmundsson, L., Seneviratne, S. I., Andrijevic, M., Frieler, K., Emanuel, K., Geiger, T., Bresch, D. N., Zhao, F., Willner, S. N., Büchner, M., Volkholz, J., Bauer, N., Chang, J., Ciais, P., Dury, M., François, L., Grillakis, M., Gosling, S. N., Hanasaki, N., Hickler, T., Huber, V., Ito, A., Jägermeyr, J., Khabarov, N., Koutroulis, A., Liu, W., Lutz, W., Mengel, M., Müller, C., Ostberg, S., Reyer, C. P. O., Stacke, T., and Wada, Y.: Intergenerational inequities in exposure to climate extremes, Science, 374, 158–160, <https://doi.org/10.1126/science.abi7339>, 2021.
- UN Department of Economic and Social Affairs: World urbanization prospects: the 2018 revision, research report, <https://population.un.org/wup/publications/Files/WUP2018-Report.pdf>, last accessed on 21 January 2024, 2019.
- Westerholt, R.: Exploratory statistical analysis of spatial structures in urban datasets, in: Metropolitan Research: Methods and Approaches, edited by Gurr, J., Parr, R., and Hardt, D., pp. 37–61, transcript, Bielefeld, Germany, <https://doi.org/10.14361/9783839463109-003>, 2022.
- Westerholt, R.: Extending the Moran scatterplot by indications of critical values and p -values: introducing the Moran semogram and the drop plot, in: Proceedings of the 32nd Annual GIS Research UK Conference (GISRUK), Leeds, UK, <https://doi.org/10.5281/zenodo.10897792>, 2024.
- Winklmayr, C., Muthers, S., Niemann, H., Mücke, H.-G., and an der Heiden, M.: Heat-related mortality in Germany from 1992 to 2021, Deutsches Arzteblatt International, 119, 451–457, <https://doi.org/10.3238/arztebl.m2022.0202>, 2022.
- World Bank: Urban population growth (annual %), last accessed on 21 January 2024, <https://data.worldbank.org/indicator/SP.URB.GROW>, 2022.
- Yuan, F. and Bauer, M. E.: Comparison of impervious surface area and normalized difference vegetation index as indicators of surface urban heat island effects in Landsat imagery, Remote Sensing of Environment, 106, 375–386, <https://doi.org/10.1016/j.rse.2006.09.003>, 2007.